Transparent, Robust and Photochemical Antibacterial Surface Based on Hydrogen Bonding Between a Silica-Alumina and Cationic Dye

Ki Joon Heo[a,b,1], Dong Uk Lee[c,1], Jae Hak Shin[d,1], Junghun Park[c], Byeong Jin Lee[c], Juhun Shin[a], Sang Bin Jeong[d], Gi Byoung Hwang[a], Alexander J. MacRobert[e], Ivan P. Parkin[a,], Jae Hee Jung[d,*] and Dong Yun Choi[c,*]*

[a]Materials Chemistry Research Centre, Department of Chemistry, University College London, WC1H 0AJ, United Kingdom

[b]School of Mechanical Engineering, Chonnam National University, Gwangju, 61186, Republic of Korea

[c]Biomedical Manufacturing Technology Center, Korea Institute of Industrial Technology, Yeongcheon, 38822, Republic of Korea

[d]Department of Mechanical Engineering, Sejong University, Seoul 05006, Republic of Korea

[e]UCL Division of Surgery and Interventional Science, Royal Free Campus, London, NW3 2PF, United Kingdom

KEYWORDS: Visible light; Antimicrobial; Photochemical disinfection; Sol-gel; Antimicrobial film

ABSTRACT

Healthcare-associated infections can occur and spread through direct contact with contaminated fomites in a hospital, such as mobile phones, tablets, computer keyboards, doorknobs, and other surfaces. Herein, this study shows a transparent, robust, and visible-light-activated antibacterial surface based on hydrogen bonds between a transparent silica-alumina (Si-Al) sol-gel and a visible-light-activated photosensitizer, such as crystal violet (CV). The study of the bonding mechanisms revealed that hydrogen bonding predominantly occurs between the N of CV and Al-OH. Apart from CV, Si-Al can be combined with a variety of dyes, highlighting its potential for wide application. The Si-Al@CV film selectively generates singlet oxygen using ambient visible light, triggering potent photochemical antibacterial performance against Gram-positive and Gram-negative bacteria. Additionally, the Si-Al@CV film is stable even after mechanical stability tests such as tape adhesion, scratch, bending and water immersion. *In vitro* cytotoxicity tests using C2C12 myoblast cells showed that the Si-Al@CV film is a biocompatible material. This work suggests a new approach for designing a transparent and robust touchscreen surface with photochemical antibacterial capability against healthcare-associated infections.

■ INTRODUCTION

Healthcare-associated infections (HAIs), which are infections acquired by patients during their stay in a hospital or another healthcare setting, are an ongoing global public health.[1] The European Centre for Disease Prevention and Control (ECDPC) estimates that over 8.9 million people suffer HAIs every year in Europe.[2] In addition, the development of antibiotic-resistant bacteria in hospitals is expected to become a more serious problem, which can lead to the incidence of related diseases.[3-6] Antibiotic-resistant bacteria such as methicillin-resistant *Staphylococcus aureus*

(MRSA) and Gram-negative *Pseudomonas aeruginosa* have been classified as "Serious Threat" by the US Centre for Disease Control (CDC).[7]

HAIs can occur and spread through direct contact with contaminated fomites in a hospital, such as mobile phones, tablets, computer keyboards, doorknobs, and other surfaces.[8] They can act as both a source and reservoir for HAIs because microorganisms can survive on these surfaces for long periods of time.[9] The use of touchscreens has become common, but they are attracting attention as a potential vector of HAIs.[10] The touchscreen surfaces of mobile phones are particularly "high risk" surfaces because they allow direct contact with the face or mouth during a call, which can be hazardous even if the hands are properly washed and clean.[11-12] In addition, mobile phones are the most frequently touched surfaces.[13] A recently published literature showed that mobile phone contamination rates range from 40% to 60%, with MRSA being the most frequently observed bacterium (10–90%).[14] Another study reported that 10% of test phones were contaminated with viral pathogens.[15]

In general, good hand hygiene and surface cleaning with disinfectants, such as ethanol sanitizer, are effective ways to prevent HAIs. A significant drawback of these traditional methods is that they are effective only at the moment of sterilization; however, the contamination of hospital surfaces is frequent and persistent.[16] To overcome this limitation, antibacterial surfaces along with silver or copper nanoparticles are being studied as an alternative approach to reducing infection from fomites. Behzadinasab *et al*. introduced a transparent antibacterial surface coating using polydopamine and Cu or Cu_2O particles that simultaneously showed potent antibacterial performance and transparency.[17] Hosseini et al. also described transparent antibacterial surfaces with silver oxide particles and silicate matrix.[18] However, these technologies can only kill microorganisms in direct contact with antibacterial substances, such that a gradual decrease in

antibacterial performance is inevitable due to the accumulation of dust or dead cells covering the functional particles. In addition, the use of inorganic nanoparticles is regulated within the EU because they can also exert adverse effects on human health.[19,20] Thus, non-harmful and real-time disinfection of surrounding touchscreen surfaces is essential for protecting public health against HAIs.

Photodynamic therapy, which uses a photosensitizer and light energy, has gained considerable attention as a promising solution for HAIs.[21,22] Antibacterial methods based on reactive oxygen species (ROS) are easy to implement and use because the only requirement is an abandoned visible light (sunlight or the indoor lights of a healthcare facility). When exposed to a light source, the photosensitizer generates various ROS, for a multisite attack that kills bacteria without the development of antibiotic-resistant of microorganisms. ROS can eliminate even dead cells and effectively kill bacteria, not in direct contact with the antibacterial substrates.[23] However, developing a transparent and visible light-activated antibacterial surface remains a challenge, because the process of coating the colored photosensitizer makes the surface opaque.[24]

To achieve a transparent light-activated antibacterial surface, it uses a new strategy with silica-alumina (Si-Al), a robust, transparent porous surface on which photosensitizer can be immobilized while maintaining potent antimicrobial performance. The transparent antibacterial surface was easily fabricated with a Si-Al sol-gel and visible-light absorbing cationic dyes including crystal violet (CV), through a one-step blade coating process conducted at room temperature. The N of the cationic dye formed strong hydrogen bonds with the OH group of the Si-Al, resulting in homogenous immobilization of the cationic dye; this increased the transparency of the surface. CV is the one example of the possible extension of the Si-Al sol-gel. The Si-Al sol-gel can be used with a variety of dyes as binder materials. It demonstrated that this transparent antibacterial surface

had a potent antibacterial performance against Gram-positive bacteria (*Staphylococcus epidermidis*) and Gram-negative bacteria (*Escherichia coli* and *Pseudomonas Syringae)* under visible light illumination and revealed the visible-light-activated antibacterial mechanism of the Si-Al@CV film. In addition, the Si-Al@CV film showed mechanical stability against tape adhesion, scratch and bending, indicating its potential use in real environments. This work is expected to present a new approach for designing and realizing practical easy-to-clean transparent antibacterial surfaces against HAIs.

■ MATERIALS AND METODS

Preparation of the Si-Al@CV coating solution. The Si-Al sol-gel solution was prepared from methyltrimethoxysilane (MTMS; 95%; Sigma-Aldrich, USA), 3-Glycidyloxypropyl) trimethoxysilane (GPTMS; 97%; Sigma-Aldrich) and aluminium tri-sec butoxide (ATSB; 99%; Sigma-Aldrich). First, alumina sol was prepared by adding ATSB (20 g) and acetylacetone (5.4 g; 99%; Sigma-Aldrich) to 2-propanol (5.4 g; IPA; 99.5% anhydrous, Sigma-Aldrich) and vigorously stirring at 80 ºC (Figure S1). In a second beaker, silica sol was prepared by adding MTMS (30 g) to GPTMS (17.3 g), mixed with IPA (34 g). Subsequently, alumina sol (21 g) and deionized water (37 g) were added to silica sol. The mixture solution was refluxed at 80 ºC for 12 h and aged at 25 ºC for over 24 h. The Si-Al@CV coating solution was prepared with various Si-Al sol-gel concentrations in anhydrous ethanol (99.9%; DUKSAN, South Korea). Then, CV (5 mM; Sigma-Aldrich) was mixed with diluted Si-Al sol-gel solution under steady agitation to completely dissolve the CV.

Preparation of the antibacterial film. All polyethylene terephthalate (PET) film was cleaned successfully with acetone, ethanol, and isopropyl alcohol in an ultrasonic cleaning bath for 15 min

each and dried at 50 ºC in a convection oven. The antibacterial film (20 mm × 20 mm) was prepared at 25 ºC by blade coating at a speed of 5 mm s^{-1}, with a gap between blade and substrate of 250 μm (blade angle of 30º) (Figure S2). The specimen coated with the Si-Al@CV solution by the blade coater was then cured at room temperature (25 ºC) for 4 h or 50 ºC in a convection oven for 2 h.

Characterization of the film surface. The surface of the Si-Al@CV film was characterized by an XPS device (NEXSA, Thermo Fisher Scientific) with an Al K-alpha source (1,486.6 eV) and an angle of 90º. To analyze the surface of the transparent antibacterial film, we performed attenuated total reflection-FTIR spectroscopy (ALPHA-P; Bruker, USA) using a diamond crystal kit. Each specimen was analyzed over 32 scans with a resolution of 4 cm^{-1}, providing spectra in the range of 600-4,000 cm^{-1}. To characterize the morphology of the films, SEM (SU8230, Hitachi, Japan) image analysis was performed at an accelerating voltage of 5 kV. The surface hardness test of the Si-Al@CV film was conducted using a pencil hardness tester (COAD.607, Ocean Science, Republic of Korea) and pencils of various hardness (3H–9H, Mitsubishi Uni, Japan). To measure the residual organic solvents in the Si-Al@CV film, VOCs were measured using a GC-MS (Qp 2010 plus, Shimadzu, Japan). The Si-Al@CV film was cut to a size of 4 × 4 cm and stored in a sealed container. Further, the sealed container was heated at 60 ºC in a convection oven for 1 h, after which the gas in the sealed container was captured to measure the VOCs via GC-MS.

Antibacterial test. The visible-light-activated antibacterial performance of the Si-Al@CV film was tested using the Gram-positive bacteria, *S. epidermidis* (KCTC 1917), and Gram-negative bacteria, *E. coli* (KCTC 1039) and *P. syringae* (DSM-21482).[25,26] All bacteria were incubated in a nutrient broth (Becton Dickinson, USA) at 37 ºC in a shaking incubator. After 18 h of culture, the bacteria were harvested through centrifugation (4,000 × g, 15 min), washed using phosphate-

buffered saline (PBS; 10 mL) to remove nutrient broth, and then centrifuged to obtain ~10^8 colony-forming unit CFU mL^{-1} bacterial suspended in PBS (10 mL). Then, bacterial suspension (25 µL) was inoculated onto PET, Si-Al, and Si-Al@CV surfaces in a moisture box with a transparent glass cover. The samples were exposed to an LED lamp (CLA60 9.5 W; 400–800 nm wavelength; Osram, Germany) from a distance of 50 mm (intensity of 7.2 mW cm^{-2}), while the same set of samples was kept in the dark box.[27,28] The samples were placed in 10 mL PBS, and vortexed for 1 min to extract bacteria from the sample into the PBS solution. After serial dilution, *S. epidermidis* and *E. coli* suspensions were placed onto a nutrient agar plate and cultured at 37 ºC for 24 h. The bacterial colonies were then counted. Each experiment included two technical replicates and each experiment was reproduced three times.

Characterization of the visible-light-activated photochemical process PL spectra were measured at a wavelength of 600–800 nm using a steady-state PL spectrometer (FluoroMax; Horiba Scientific, USA) with a 540 nm excitation wavelength. Singlet oxygen phosphorescence was measured at a wavelength of ~1,270 nm using a near-infrared sensitive thermoelectrically cooled photomultiplier and a PC-mounted multi-scaler board with a pre-amplifier (MSA-300, Becker-Hickl, Germany). The test film was placed onto a slide glass and irradiated by an Nd:YAG laser operating at 532 nm. The data were then analyzed using FluoFit software (PicoQuant GmbH, Germany).

Determination of the key ROS leading to bacterial inactivation. Scavengers and quenchers of ROS, including catalase, L-histidine, mannitol, and superoxide dismutase, were purchased from Sigma-Aldrich and used with an *S. epidermidis* suspension (~3.0×10^6 CFU mL^{-1}). Then, catalase (6–14 units mL^{-1}), L-histidine (2 mM), mannitol (82 mM), and superoxide (20 units mL^{-1}) in the *S. epidermidis* suspension were used as a hydrogen peroxide scavenger, singlet oxygen quencher,

hydroxyl radical scavenger, and superoxide radical scavenger, respectively.[27,28] The Si-Al@CV films were submerged in each bacterial suspension containing ROS scavenger or quencher and then exposed to visible light at an optical power of 7.2 mW cm^{-2} for 6 h. After a serial dilution, bacterial suspension (100 µL) was inoculated onto a nutrient agar plate and cultured at 37 ºC for 24 h. The bacterial colonies grown in the agar plate were then counted.

Dye leaching test. The Si-Al@CV films were cut to 3 × 3 cm portions and dipped into DI water (10 mL) for 1 to 14 days to confirm the CV leaching. In addition, the Si-Al@CV films were soaked in 10 mL of a pH 10 aqueous solution (Sodium carbonate buffer) and water with detergent (commercial detergent, 0.2 vol%). The solution of leached CV dye was measured via UV-Vis spectroscopy (JP/UV-3600, Shimadzu, Japan) and the concentration was calculated by calibration curve.

Cytotoxicity assay. The in vitro cytotoxicity of the Si-Al@CV film was determined using C2C12 (ATCC CRL-1772), a subclone of the mouse myoblast cell line, using the Cell Counting kit-8 (CCK-8; Dojindo Laboratories, Japan) assay.[29] The PET and Si-Al@CV films were cut to dimensions of 4 mm × 5 mm in a rectangular shape and cleaned with DI water. $NiSO_4$ (99.99%, Sigma-Aldrich, USA) was prepared at a concentration of 10 mg/mL in the culture medium as a positive control. Cells were cultured in Dulbecco's modified Eagle's medium (DMEM; Hyclone, Cat. No. SH30243, USA) supplemented with 10% fetal bovine serum (ATCC, Cat. No. 30-2020, USA) and 1% penicillin/streptomycin (Hyclone, Cat. No. SV30010, USA) at 37 °C in a humidified atmosphere containing 5% CO_2. The cells were seeded in 96-well cell culture plates at 5.0×10^3 cells per well and cultured to adhere at 37 °C for 24 h in 5% CO_2 atmosphere. After cell attachment, the cells were cultured in untreated (control), PET film, Si-Al@CV film, and $NiSO_4$ solution for 24 h. At each time point, the films were removed, and cultured cells were visually analyzed using

an optical microscope (Eclipse Ti-u; Nikon, Japan). Subsequently, the CCK-8 reagent was applied to the cells at a concentration of 1:5 (CCK-8 reagent: DMEM medium), and the cells were incubated for 4 h. Absorbance was measured at 450 nm using a microplate reader (Synergy H1, Biotek, USA). Cell viability was calculated as follows:

$$\text{Cell viability (\%)} = \frac{A_{sample} - A_{blank}}{A_{control} - A_{blank}} \times 100$$

where A_{sample} is the absorbance of the samples, A_{blank} is the absorbance of the blank (containing DMEM and CCK-8 solution), and $A_{control}$ is the untreated sample (without films). The experiments were conducted in triplicate, and data are reported as mean values with standard deviation.

■ RESULTS AND DISCUSSION

To realise a transparent and visible-light-activated antibacterial surface against HAIs, we present here an easy-to-use and transparent cationic dye binder, Si-Al sol-gel (Figure 1a and Figure S1). Silica sol-gel is a typical transparent binding material. However, it is difficult to cure at room temperature, and an additional thermal treatment process is required.[30] Figure 1b shows a digital image of Si-Al films according to the Al concentration. When only Si was used, a uniform and transparent film was not obtained. However, when 5% Al was added, a uniform transparent film was fabricated, even at room temperature, which can be attributed to the Al oxidation behaviour. Owing to the standard reduction potentials of aluminum (-1.66 V at 25℃ in air) and the lack of chelation ratio (acetyl acetone/ATSB molar ratio of 0.66), alumina formation could be induced at a relatively low temperature.[31] The scanning electron microscopy (SEM) images in Figure 1c(i) show that the film surface without Al was visibly cracked, whereas a smooth and uniform surface was observed at an Al concentration of 5% (Figure 1c(ii)). However, if the Al concentration was

too high, crystallization of the sol-gel scaffold occurred,[32] leading to the formation of particles owing to the strong oxidation behavior. When Al concentration was 10%, particles formed by oxidation of Al were confirmed (Figure 1c(iii)) and the pores formed as the Al concentration increased further increased to 20 wt% (Figure 1c(iv)). This particle formation led to the collapse of the Si–Al film transparency. The generation of particles owing to the oxidation properties of Al is clearly identified in the digital image of the solutions in Figure 1d. A Si sol-gel without Al showed transparency, and when a 5% concentration of Al was added, the color changed to yellow while maintaining the transparency. However, as the Al concentration increased, particles were generated due to the oxidation properties of Al, which induced a change in the solution state from sol to gel. In addition, the FT-IR spectra indicated that the addition of the Al sol had a synergetic effect on polymerization (Figure S2). FT-IR spectra showed that the siloxane peak increased after Al addition, and the low molecular linear siloxane (1,045 cm^{-1}) in the Si-Al solution were changed to high-molecular-weight linear siloxane (1,015 and 1,085 cm^{-1}) during the formation of the Si-Al film, indicating that the Al sol helped the polymerization of Si-Al. These results indicate that an optimized Al concentration is essential for the fabrication of transparent and smooth film surfaces, as the Al concentration determines the properties of the Si-Al nanocomposite coating surface. Therefore, to achieve both transparency and low temperature curing, the required Al concentration was determined to be 5% due to its optimal mechanical properties (Figure S3).[33]

Our previous study reported the possibility that the Si-Al sol can bind CV through hydrogen bonding, which is an electrostatic attraction.[23] The large difference in electronegativity between the H atom (partial positive charge) in Si-Al containing OH bonds and the N atom (partial negative charge) in the CV can lead to hydrogen bonding. To fully understand hydrogen bonding between Si-Al and CV, Fourier-Transform Infrared (FTIR) spectroscopy was used to characterize the main

groups of the Si-Al@CV film (Figure 2a). Unlike the uncoated PET (control) spectra, the spectra of Si-Al film showed major peaks corresponding to Si-CH_3 (1,270 cm^{-1}), Si-CH_2 (770 cm^{-1}), and Si-O-Si (Si-O-Al) stretching (1,040 cm^{-1}), and OH (Si-OH, Al-OH) stretching (3,200–3,550 cm^{-1}).[23,34] After CV modification, new peaks corresponding to the C-N stretching of aromatic tertiary amine (1,361 cm^{-1}), CV ring vibration (1,590 cm^{-1}), and C-benzene ring stretching (1,170 cm^{-1}) were observed,[35,36] indicating the presence of CV. In addition, a red-shift occurred in the OH stretching band (Figure 2b). This implies that hydrogen bonding has occurred between the OH group of Si-Al sol-gel with the N-atoms of CV.[36-39] To further understand the hydrogen bonding of Si-Al@CV, X-ray photoelectron spectroscopy (XPS) was used to examine the bonding structures and chemical composition of the films. The overall XPS survey spectra; the presence of O, C, Si, Al, and N elements in the Si-Al@CV film was revealed (Figure S4). The C 1s peak from adventitious carbon at 285.0 eV was used as an internal energy reference during the analysis (Figure 2c). Two different binding energies at 286.9 and 285.0 eV were assigned to C-O and C-C, respectively. Figure 2d shows the O 1s XPS spectra of Si-Al and Si-Al@CV film. The chemical bonding of O of Si-Al changed after CV modification; O 1s binding energy slightly decreased, with the addition of CV. The Al 2p binding energy also slightly decreased from 76.0 to 75.1 (Figure 2e). This binding energy decrease occurred because, when the OH groups in Si-Al sol and the N in CV form intermolecular hydrogen bonds, electrons moved from N to the OH groups, thereby increasing the electron density of Al-OH.[36,40] Therefore, after CV modification, the O 1s and Al 2p binding energy of Si-Al decreased due to the increase in electron density. In contrast, the N 1s binding energy of CV increased from 399.4 to 399.8, which suggested electron transfer from the N of CV to the OH group of Si-Al (Figure 2f). However, interestingly, the Si 2p XPS spectra of Si-Al did not change after CV modification (Figure 2g). To understand these results, a further XPS

analysis was conducted. When there was only Si without the addition of Al, there was also no change in O 1s and Si 2p XPS spectra after CV modification, indicating that no hydrogen bonds occurred between Si-OH and CV (Figure S5). These XPS results imply that Si-Al sol-gel and CV molecules were hydrogen-bonded and that Al has played an important role in hydrogen bonding (Figure 2h). The uniform deposition of CV is an important factor for designing a dye-coated transparent surface, as it solves the problem of surface opacity caused by the aggregation of dyes in the polymer pores during the dye coating process. Thus, homogeneous deposition of CV by hydrogen bonding can provide a new strategy for designing a dye-coated transparent surface. Additionally, CV is the only possible application of an Si-Al sol-gel. An Si-Al sol-gel can be easily applied to a variety of dyes via hydrogen bonding (Figure S6).

As shown in Figure 3a, following the Si-Al coating, the PET film maintained its color and transparency, indicating the transparency properties of Si-Al. To investigate the effect of Si-Al sol-gel coating on the PET film, bending strength measurements were performed using a bending force test device. There was no significant difference between the uncoated PET and Si-Al@CV-coated PET films in terms of bending force (Figure S7). Upon adding CV, the film remained transparent and maintained a uniform surface (Figure S8); however, the color changed to violet. This color change is reflected in the visible-light absorbing property of the dyes. Figure 3b shows the UV-vis absorbance spectra of PET, Si-Al, and Si-Al@CV film over a wavelength range of 400-700 nm (visible light region). The PET and Si-Al film did not show primary absorption, whereas the Si-Al@CV film showed a significant absorption peak at 594 nm. This light absorption enables the photoreaction of Si-Al@CV film, which is the basis for the potent antibacterial activity seen under visible-light exposure conditions. However, this light absorption property of CV deteriorated the transparency of the Si-Al@CV film. To overcome this limitation, there is a need

to determine the optimal coating conditions including the CV concentration and film thickness, to realize a transparent antibacterial surface.

A thin and uniform surface is important to achieve a transparent surface. To scrutinize the effect of film thickness on the transparency and antibacterial performance of Si-Al@CV film, Si-Al@CV films with various thicknesses were prepared by blade coating methods (meniscus assisted solution printing) (Figure S9 and Supporting Movie S1). The blade coating method is suitable for adjusting the thickness of the coating film.[41-43] As shown in Figure 3c, the coating solution passes through a thin gap between the blade and moving substrate to form a uniform coated layer. Generally, the thickness of the coating is determined by the characterizations of the solution, velocity of moving substrate, and blade angle (Figure S10).[44,45] The thickness (t) of the coating can be calculated by the Landau-Levich-Derjaguin model as follows:[46]

$$t \propto \kappa^{-1} Ca^{2/3}$$

Where κ^{-1} is the capillary length and Ca is the capillary number. The κ^{-1} estimates the relative effects of Laplace pressure and hydrostatic pressure and is defined as $\kappa^{-1} = (\gamma / \rho g)^{1/2}$. Here, γ is the surface tension of the liquid, ρ is the density of liquid, and g is the gravity. The Ca represents the ratio of viscous force to capillary force and is defined as $\mu V \gamma^{-1}$ where μ and V are the viscosity and substrate moving speed, respectively.

To evaluate the effect of film thickness, Si-Al@CV films were prepared according to the Si-Al concentrations. Figures 3d and 3e summarize the effects of the Si-Al concentration on the thickness and transparency of the Si-Al@CV film. Under a low Si-Al concentration (< 20 wt%), an unstable film was fabricated (Figure S11). When the concentration increased from 30 to 60 wt%, the thickness of the Si-Al@CV film gradually increased from 2.3 to 7.1 μm (Figure S12), while the transparency gradually decreased from 78.4% to 72.3% at 590 nm. An increase in the Si-Al content

led to an increase in the viscosity of the solution and a decrease in the amount of solvent evaporation, which resulted from an increase in thickness of the coating layer. Interestingly, film thickness had no significant effect on the antibacterial performance induced by visible light illumination (Figure 3f). These results show that the thin film fabricated by controlling film thickness played an important role in realizing a transparent antibacterial film.

Figure 4a describes the transmittance of Si-Al@CV with respect to the CV concentration. As the CV concentration increased, the color of the Si-Al@CV film gradually deepened, and the transparency in the 590 nm region consistently decreased, indicating that the CV concentration plays an important role in the transparency of the Si-Al@CV film. However, the amount of CV used cannot be unconditionally lowered because the antibacterial performance is also significantly affected by the CV concentration. Figure 4b shows the antibacterial activity of the Si-Al@CV film against *S. epidermidis* at different CV concentrations after 6 h of visible-light exposure (Figure S13). At concentrations < 1 mM, no relationship between the antibacterial performance and CV concentration was observed, except for the natural decay occurring due to the bacteria being exposed to air. However, at concentrations > 1 mM, potent bactericidal performance (> 2.9 log reduction) was observed. Therefore, to obtain a transparent antibacterial surface, the optimal CV concentration was determined to be 1 mM (Figure S14). Figure 4c demonstrates that antibacterial activity was only exerted under light conditions with 1mM CV, indicating that the antibacterial activity of Si-Al@CV was primarily influenced by the visible-light-activated inactivation reaction induced by CV. This result is consistent with previous finding that antibacterial activity at the low concentrations of CV-coated surface was only observed when they were exposed to light.[47]

Figure 4d shows the photochemical antibacterial mechanism of CV under illumination. First, the CV (photosensitizer) molecules absorb photons from the light source to form excited singlet states,

which then return to the ground state or transform into an excited triplet state. The excited triplet state triggers ROS generation. The excited triplet state can transfer electrons to molecular oxygen to generate free radicals (Type I, redox reaction), or transfer its energy to a ground-state triplet oxygen to generate excited singlet oxygen (Type II, energy transfer). The generated ROS attacks the cell, leading to cell death. Further analyses were conducted to fully understand the visible-light-activated photochemical bactericidal mechanism. Figure 4e shows the photoluminescence (PL) spectra of the PET, Si-Al, and Si-Al@CV surfaces from 600 to 800 nm. When the excited singlet states returned to the ground state, the PL appeared to lose energy; therefore, the PL spectra indicated that the molecules reacted with light. Si-Al did not significantly change in the PL spectra, indicating that it did not react with light. Contrastingly, the PL spectrum of Si-Al@CV clearly shows that it was excited by light. To confirm the ROS generation of Si-Al@CV, $^1O_2$ phosphorescence decay was measured at a wavelength of 1,270 nm (Figure 4f). After laser exposure, the $^1O_2$ phosphorescence signal was observed on Si-Al@CV and the lifetime of the phosphorescence signal was 48.0 μs, indicating that Si-Al@CV produced $^1O_2$ upon illumination. This result supported previous findings that type II mechanism is energetically available for CV dye, indicating that CV can acts as a photosensitizer to generate ROS using visible light.[48]

To determine the ROS responsible for the bactericidal effect of Si-Al@CV, ROS-scavenger quenching assays were performed (Figure 4g). After adding the $^1O_2$ quencher L-histidine, the antibacterial performance of the Si-Al@CV film decreased to 0.2 log reduction, indicating a complete loss of bacterial activity. These results indicate that Si-Al@CV reacts with visible light to generate $^1O_2$, which is the key ROS leading to bacterial inactivation, and it is consistent with previous antibacterial mechanism studies on CV-coated surfaces.[23,48] However, the antibacterial mechanism of Si-Al@CV differed from that of previous studies, in which the antibacterial activity

of CV was attributed to the simultaneous occurrence of ROS via both Type 1 and Type 2 mechanisms. Sehmi *et al.* demonstrated that the $^1O_2$ scavenger dominantly affected the bactericidal activity of CV-coated polyurethane against *E. Coli*. Furthermore, the H_2O_2 scavenger significantly reduced bactericidal activity.[49] Jeong *et al*. also reported that although $^1O_2$ was the main contributor to the death of *S. epidermidis*, the antibacterial activity of the CV-coated surface decreased after O_2^- removal.[23] However, the Si-Al@CV film showed an insignificant change in antibacterial activity compared to the no scavenger condition when •OH, O_2^- and H_2O_2 were scavenged by the addition of catalase, mannitol, and superoxide dismutase, respectively. This result suggests that Si-Al@CV can selectively generate ROS through only Type II mechanisms. It can be explained that the Si-Al sol-gel matrix may have acted as an insulator that was undesirable for the electron transfer reaction, thereby suppressing the Type I reaction and primarily expressing the Type II pathway.The Type II process is a desirable mechanism because the lifetime of singlet oxygen generated by Type II in the air is longer (~2.8s) than other ROS, and during this time, it can diffuse by approximately 1 cm.[50] This indicates the possibility of more effective sterilization despite surface contamination such as human oil and dust deposition or indirect contact with bacteria. Figure 4h shows the an antibacterial activity of Si-Al@CV film after fingerprnit contamination. Antibacterial activity (>2.9 log reduction) remained even after the surface was fully contaminated by fingerprints (~100 times) (Figure S15).

In addition, the selective Type II reaction can return CV to its ground state to enable the regeneration of $^1O_2$ after producing $^1O_2$, thereby reducing the self-photodegradation of CV. It suggests the possibility of extending the stability of organic dyes. Nevertheless, despite this selective type II reaction, the antibacterial activity of Si-Al@CV decreased over time to a 1.2 log reduction after 5 d (Figure S16). **This** may be the result of generated ROS-induced self-

photodegradation. Therefore, the possibility of a transparent photochemical antibacterial film with antibacterial activity lasting more than 5 d has been demonstrated, but further research is required to overcome ROS-induced self-photodegradation for the practical application of the Si-Al@CV film in everyday life.

Furthermore, our previous study demonstrated that Si-Al with 1H, 1H, 2H, 2H-perfluorooctyltriethoxysilane (PFOTES) promoted the Type I reaction of CV while simultaneously attenuating the Type II reaction.[23] This difference may be due to the presence of fluorine on the surface of PFOTES. It is well known that surface fluorination increases the photogeneration of •OH and reduces the recombination rate of electron-hole pairs. Fluorination can trap CV electrons because of the high electronegativity of fluorine, thus accelerating O_2 reduction.[51] This result implies that ROS generation can be controlled by combining Si-Al@CV with other materials. Although Si-Al could selectively control the photochemical reaction with CV, it may not be effective for all cationic dyes. Therefore, additional research is needed to confirm the control of ROS generation by Si-Al.

To evaluate the visible light-activated antibacterial performance of Si-Al@CV, further studies were conducted on gram-negative bacteria (*E. coli* and *P. syringae*) (Figure S17). Si-Al@CV had a potent antibacterial performance against *E. coli* (~1.4 log reduction) and *P. syringae* (~1.1 log reduction) but was not as effective against *S. epidermidis* (~ 2.9 log reduction). The difference in antibacterial performance is attributed to the dissimilar cell structures and physiologies of Gram-positive and Gram-negative.[52] Gram-positive bacteria have a thick peptidoglycan layer with a high degree of porosity, which allows ROS to reach the cytoplasmic membrane more easily.[53] However, Gram-negative bacteria have a more complex cell wall layer composed of a relatively thin peptidoglycan cell wall and an additional bacterial outer membrane, which play an important role

in reducing the permeability of many molecules and resisting antibacterial agents.[54-56] These results highlight the outstanding photochemical inactivation effect of Si-Al@CV on various microbes.

In the real world, touchscreen surfaces are inevitably and continuously exposed to various types of contact and wear. Another favorable property of the Si-Al@CV films is mechanical stability. It was tested by measuring the adhesion of the double-sided tape, scratching, and bending.[57] Figure 5a shows the absorbance of Si-Al@CV at 594 nm after tape peeling (A) compared to the absorbance of the initial film (A_o). After 60 tape peeling cycles, the film surface remained stable (Supporting Movies S2), indicating that the tape peel-off did not affect the surface stability. Additionally, the surface was intact with no cracks when bent at a bending radius of 0.5 mm (Figures 5b and S18), suggesting its potential applicability to flexible or rollable surfaces. A pencil hardness test was performed to determine stability against scratching (Figure 5c). The Si-Al@CV film obtained a hardness of 5H, which was higher than the 4H of the PET film substrate. Therefore, as shown in Supporting Movies S3, the film surface remained stable after scratching. In addition, the antibacterial activity of Si-Al@CV remained after bending or scratching (Figure S19). Our study showed that the Si-Al@CV film tolerated prolonged abrasion tests without damaging its surface properties, implying its practical applicability to frequently touched surfaces.

Because touch screens are typically exposed to water, such as sweat or wet tissue, moisture resistance is important. To determine the stability of the Si-Al@CV film against water, the sample was immersed in deionized water and the absorbance at 590 nm was periodically measured via UV-vis spectrometry for 14 days. As shown in Figure 5d, after 24 h of immersion, negligible leaching (~3.0 ppb) of CV was detected, and no additional leaching was observed. The total amount of CV leached out from Si-Al@CV was < 0.045%, indicating almost complete stability.[51]

Even when exposed a pH 10 or detergent-containing water conditions, the Si-Al@CV film was stable. (Figure S20). In addition, the antibacterial activity of Si-Al@CV remained after exposure to water (Figure S21). These results indicate that the Si-Al@CV film was resistant to water exposure. The Si-Al@CV film exhibited excellent stability against ethanol (Supporting Movie S4), which is commonly used for disinfection and cleaning. Owing to its stability, the Si-Al@CV film could be easily cleaned using wipers or water flow when the surface was contaminated (Figure 5e and Supporting Movie S5). Although the stability of Si-Al@CV against water exposure was demonstrated, it is necessary of further studies to determine the stability of Si-Al@CV against exposure to various solutions.

Safety related to the biotoxicity of materials must be verified, for them to be applied to a practical touch screen that has direct contact with the skin. Although the stability of the Si-Al film was demonstrated through a stability test, exposure to Si-Al@CV by accidental damage to the film will cause skin injuries if Si-Al@CV is toxic to human skin. Therefore, to evaluate the biosafety of Si-Al@CV, the biocompatibility of the Si-Al@CV film was investigated using an in vitro cytotoxicity assay with C2C12 myoblast cells (Figure S22). To minimize physical damage to the cells during cell culture, the films were immersed obliquely in the culture medium in the well plate. For the assay, a non-treated condition was employed as an assay control, while PET film and nickel sulfate ($NiSO_4$) were used as negative control and positive control, respectively.[58] The Si-Al@CV film and control samples were applied to each well from 1 h to 24 h. Figure 6a shows the cell viability results of the test sample with controls. It can be observed that the Si-Al@CV showed cell viability (101.4%) similar to that of the control group for 24 h incubation; contrastingly, very low cell viability was obtained with positive control (5.9%). Additionally, Figures 6b and S23 show optical cell images under experimental conditions, indicating that the Si-Al@CV film does not affect cell

adhesion and growth. Furthermore, to evaluate the residual organic solvents used in the manufacturing process of Si-Al@CV, volatile organic solvents (VOCs) were measured by gas chromatography mass spectrometer (GC-MS). The Si-Al@CV film was stored in a sealed container, and the sealed container was heated to 60 °C, and then gas in the sealed container was measured. A low concentration of organic solvents (~0.2 ppm) was released from the Si-Al@CV film, indicating that organic solvents were completely removed during the fabrication process (Figure S24). Therefore, it was confirmed that the Si-Al@CV film is a biocompatible material and can provide experimental support for the potential application of the Si-Al@CV film in real life, without toxicity.

Figure 6c shows an example of the application of the Si-Al@CV film to the commercial touchscreen of a smartphone. Following the installation, the Si-Al@CV film on the smartphone screen was maintained owing to the robust and flexible properties of the Si-Al@CV film (Supporting Movie S6). The touchscreen colors remained unchanged after the Si-Al@CV film was attached. Furthermore, the screening function was retained using the Si-Al@CV film. These results indicate that the Si-Al@CV film can effectively impart antibacterial performance while maintaining the functional properties of the touchscreen surface, highlighting its feasibility for practical applicability in real-environment touch screens (Figure 6d).

From an engineering perspective, this Si-Al@CV sol-gel can also be applied to curved substrates (Figure 6e) and is scalable using various alternative coating methods. As one of the most frequently touched surfaces, the smartphone case often has high bacterial contamination in the healthcare environment; however, owing to its complex three-dimensional structure, coating it using a blade-coating method is challenging. Figures 6f and S25 show the applicability of the Si-Al@CV coating to a smartphone (Samsung Galaxy Note 20 Ultra) with the air spray method performed using an

airbrush device (BBA-003, Yamato Comp, Republic of Korea). Even when coated with the spray, both the transparency and stability of Si-Al@CV were maintained, indicating its applicability for surfaces of various shapes, including curved door handles.

■ CONCLUSION

To summarize, this study introduces a new strategy for a transparent and robust antibacterial film, Si-Al@CV, that is photochemically reactive to visible light. The Si-Al sol-gel is easy to fabricate transparent and can form a robust film at low temperatures by the oxidation of Al. A CV molecule is strongly immobilized within the Si-Al sol-gel matrix by hydrogen bonding between the N atoms of the CV molecule and OH bonds of the Al. CV is only one possible agent that can be used with the transparent Si-Al binder. A Si-Al binder can be combined with a variety of dyes through hydrogen bonding. The transparent antibacterial Si-Al@CV film is fabricated by exploiting the interaction between the optimized CV concentration and uniform thin film created by the blade coating method. The Si-Al@CV films effectively inactivated both Gram-positive and -negative bacteria due to the $^1O_2$ generated by the visible-light-activated photochemical reaction of CV. In addition, it confirmed the stability of the Si-Al@CV film following scratching, tape adhesion, bending, and soaking in water, and did not detect any film detachment. This stability allowed surface contamination to be easily removed using common cleaning methods, such as cleaning with water or wiping with a tissue. Cytotoxicity test using C2C12 myoblast cells revealed that Si-Al@CV is a biocompatible material without toxicity, highlighting the practical applicability of Si-Al@CV films. Furthermore, it demonstrated the potential use of the Si-Al@CV film as a transparent antibacterial screen protector while maintaining screen function. Thus, this research

provides a new direction for the realization of practical transparent antibacterial surfaces against HAIs.

■ ASSOCIATED CONTENT

Supporting information

The Supporting Information is available free of charge on the ACS Publication website.

Schematic scheme for the preparation of Silica-Alumina (Si-Al) sol-gel. Author Information (Figure S1), FT-IR spectra of Al addition. (a) Film and solution of Si-Al@CV (Figure S2), Thermogravimetric analysis (TGA) of Si–Al coatings with various Al contents (Figure S3), Overall XPS survey of the control, Si-Al, and Si-Al@CV film (Figure S4), X-ray photoelectron spectroscopy (XPS) spectra of Si and Si@crystal violet (CV) film (Figure S5), Digital image of a transparent antibacterial film with toluidine blue O (TBO), rose bengal (RB), methylene blue (MB), and CV dyes (Figure S6), Changes in mechanical property according to Si-Al@CV coating (Figure S7), Surface morphology measured by SEM and AFM (Figure S8), Photograph of the blade coating system (Figure S9), The transmittance of Si-Al@CV film at different conditions (Figure S10), Digital images of Si-Al@CV film according to Si-Al concentration (Figure S11), Cross-sectional scanning electron microscope (SEM) images of the Si-Al film thickness according to Si-Al sol concentration (Figure S12), Spectrum of LED light used in this paper (Figure S13), Digital image of the coating solution (Figure S14), Image of Si-Al@CV surface according to the number of fingerprint contacts (Figure S15), The antibacterial activity of Si-Al@CV film against *S. epidermidis* after 120 h of light exposure (Figure S16), Antibacterial performance of Si-Al@CV film against Gram-negative bacteria (Figure S17), SEM images of Si-Al film surface after being bent with a 0.5 mm radius of curvature depending on Al concentration (Figure S18), The stability

of antibacterial activity of Si-Al@CV film against mechanical wear (Figure S19), UV-Vis spectra of the soaking test results detergent and water solution of pH 7 and 10 (Figure S20), The antibacterial activity of Si-Al@CV against *S. epidermidis* according to washing (Figure S21), Test protocol of cytotoxicity test (Figure S22), Cell images of the control, PET, Si-Al@CV, and $NiSO_4$ after 0 and 24 h exposure (Figure S23), GC-MS analysis via volatile organic solvents measuring process (Figure S24), Flexible smartphone case using the transparent antibacterial film (Figure S25) (PDF)

Meniscus blade coating process of Si-Al@CV coating (Movie S1), Durability of Si-Al@CV film against tape adhesion test (Movie S2), Durability of Si-Al@CV film against surface scratch test (Movie S3), Durability of Si-Al@CV film against wiping test with ethanol solvent (Movie S4), Washability test of Si-Al@CV film (Movie S5), Retained touch screen function with the Si-Al@CV film on smartphone (Movie S6)

■ AUTHOR INFORMATION

Corresponding Author

***E-mail:** i.p.parkin@ucl.ac.uk (I.P. Parkin), jaehee@sejong.ac.kr (J.H. Jung), dychoi311@kitech.re.kr (D.Y. Choi)

Author Contributions

Ki Joon Heo: Carried out Conceptualization, Investigation, Methodology, Writing – original draft.

Dong Uk Lee: Carried out Conceptualization, Visualization, Investigation, Methodology, Writing – original draft.

Jae Hak Shin: Investigation, Data Curation, Methodology, Writing – original draft.

Junghun Park: Carried out Data Curation, Visualization, Methodology.

Byeong Jin Lee: Carried out Data Curation, Formal analysis.

Juhun Shin: Carried out Investigation, Formal analysis.

Sang Bin Jeong: Carried out Investigation, Resources, Formal analysis.

Gi Byoung Hwang: Carried out Formal analysis, Investigation.

Alexander J. MacRobert: Carried out Validation, Methodology, Investigation.

Ivan P. Parkin: Carried out Supervision, Writing -review & editing.

Jae Hee Jung: Carried out Supervision, Funding acquisition, Writing -review & editing.

Dong Yun Choi: Carried out Conceptualization, Supervision, Funding acquisition, Writing -review & editing.

Notes

The authors declare that they have no known competing financial interests or personal relationships that could have appeared to influence the work reported in this paper.

Acknowledgment

This work was supported by the National Research Foundation of Korea (NRF) grant funded by the Korea government (MSIT) (2022R1F1A1074255, 2021R1A6A3A03044302, and 2022R1A2B5B02001231). It was also partly supported by the Basic Research Fund (NK231A) from the Korea Institute of Machinery and Materials, and the Institutional Program of the Korea Institute of Industrial Technology (KITECH EO-22-0002). G.B.H. is grateful to the Ramsay Memorial Trust and UCL Chemistry for their support.

■ References

(1) World Health Organization, "*Report on the burden of endemic health care-associated infection worldwide*.", 2011. https://www.who.int/publications/i/item/report-on-the-burden-of-endemic-health-care-associated-infection-worldwide

(2) European Centre for Disease Prevention and Control (ECDPC), " Infographic: Healthcare-associated infections – a threat to patient safety in Europe", 2018. https://www.ecdc.europa.eu/en/publications-data/infographic-healthcare-associated-infections-threat-patient-safety-europe

(3) Weiner-Lastinger, L. M.; Abner, S.; Edwards, J. R.; Kallen, A. J.; Karlsson, M.; Magill, S. S.; Pollock, D.; See, I.; Soe, M. M.; Walters, M. S.; Dudeck, M. A.; Antimicrobial-resistant pathogens associated with adult healthcare-associated infections: summary of data reported to the National Healthcare Safety Network. *Infect. Control Hosp. Epidemiol.* **2020,** *41(1)*, 1-18. DOI: 10.1017/ice.2019.296.

(4) Suetens, C.; Latour, K.; Kärki, T.; Ricchizzi, E.; Kinross, P.; Luisa Moro, M.; Prevalence of healthcare-associated infections, estimated incidence and composite antimicrobial resistance index in acute care hospitals and long-term care facilities: results from two European point prevalence surveys, 2016 to 2017. *Eurosurveillance* **2018**, *23(46)*, 1800516. DOI: 10.2807/1560-7917.ES.2018.23.46.1800516.

(5) Klein, E.; Smith, D. L.; Laxminarayan. R.; Hospitalizations and Deaths Caused by Methicillin-Resistant Staphylococcus aureus, United States, 1999–2005. *Emerg. Infect. Dis.* **2007**, *13(12)*, 1840-1846. DOI: 10.3201/eid1312.070629.

(6) Chouhan, N.; Hait, M.; Roymahapatra, G.; Huang, M.; Xu, B. B.; Guo, Z.; Complexation of Antibiotics with Transition Metal Ions: A Review. *ES Food & Agroforestry* **2022**, *8*, 1-11. DOI: 10.30919/esfaf665

(7) Kadri, S. S.; Key Takeaways From the U.S. CDC's 2019 Antibiotic Resistance Threats Report for Frontline Providers. *Crit. Care Med.* **2020**, *48(7)*, 939.-945. DOI: 10.1097/CCM.0000000000004371.

(8) Adlhart, C.; Verran, J.; Azevedo, N. F.; Olmez, H.; Keinänen-Toivola, M. M.; Gouveia, I.; Melo, L.F.; Crijns, F.; Surface modifications for antimicrobial effects in the healthcare setting: a critical overview. *J. Hosp. Infect.* **2018**, *99(3)*, 239-249. DOI: 10.1016/j.jhin.2018.01.018.

(9) Imani, S. M.; Ladouceur, L.; Marshall, T.; Maclachlan, R.; Soleymani, L.; Didar, T. F.; Antimicrobial nanomaterials and coatings: current mechanisms and future perspectives to control the spread of viruses including SARS-CoV-2. *ACS Nano* **2020**, *14(10)*, 12341-12369. DOI: 10.1021/acsnano.0c05937.

(10) Panigrahi, S. K.; Pathak, V. K.; Kumar, M. M.; Raj, U.; Priya, P. K.; Covid-19 and mobile phone hygiene in healthcare settings. *BMJ Glob. Health* **2020**, *5(4)*, e002505. DOI: 10.1136/bmjgh-2020-002505.

(11) Olsen, M.; Campos, M.; Lohning, A.; Jones, P.; Legget, J.; Bannach-Brown, A.; McKirdy, S.; Alghafri, R.; Tajouri, L.; Mobile phones represent a pathway for microbial transmission: A scoping review. *Travel Med. Infect. Dis.* **2020**, *35*, 101704. DOI: 10.1016/j.tmaid.2020.101704.

(12) Trivedi, H. R.; Desai, K. J.; Trivedi, L. P.; Malek, S. S.; Javdekar, T. B.; Role of mobile phone in spreading hospital acquired infection: a study in different group of health care workers.

Natl. J. Integr. Res. Med. **2011**, *2(3)*, 56-61. http://nicpd.ac.in/ojs-/index.php/njirm/article/view/1922

(13) Cavari, Y.; Kaplan, O.; Zander, A.; Hazan, G.; Shemer-Avni, Y.; Borer, A.; Healthcare workers mobile phone usage: A potential risk for viral contamination. Surveillance pilot study. *Infect. Dis.* **2016**, *48(6)*, 432-435. DOI: 10.3109/23744235.2015.1133926.

(14) Corrin, T.; Lin, J.; Macnaughton, C.; Mahato, S.; Rajendiran, A.; The role of mobile communication devices in the spread of infections within a clinical setting. *Environ. Health Rev.* **2016**, *59(2)*, 63-70. DOI: 10.5864/d2016-014.

(15) Cassidy, S. S.; Sanders, D. J.; Wade, J.; Parkin, I. P.; Carmalt, C. J.; Smith, A. M.; Allan, E.; Antimicrobial surfaces: A need for stewardship?. *PLOS Pathog.* **2020**, *16(10)*, e1008880. DOI: 10.1371/journal.ppat.1008880.

(16) Chen, Y.; Sheng, W.; Wang, J.; Chang, S.; Lin, H.; Tien, K.; Hsu, L.; Tsai, K.; Effectiveness and limitations of hand hygiene promotion on decreasing healthcare–associated infections. *PLoS One* **2011**, *6(11)*, e27163. DOI: 10.1371/journal.pone.0027163.

(17) Behzadinasab, S.; Williams, M. D.; Hosseini, M.; Poon, L. L. M.; Chin, A. W. H.; Joseph, O. F.; Ducker, W. A.; Transparent and Sprayable Surface Coatings that Kill Drug-Resistant Bacteria Within Minutes and Inactivate SARS-CoV-2 Virus. *ACS Appl. Mater. Interfaces* **2021**, *13(46)*, 54706-54714. DOI: 10.1021/acsami.1c15505.

(18) Hosseini, M.; Chin, A. W. H.; Williams, M. D.; Behzadinasab, S.; Falkinham, J. O.; Leo, L. M.; Ducker, W. A.; Transparent Anti-SARS-CoV-2 and Antibacterial Silver Oxide Coatings. *ACS Appl. Mater. Interfaces* **2022**, *14(7)*, 8718-8727. DOI: 10.1021/acsami.1c20872.

(19) Hofmann-Amtenbrink, M.; Grainger, D. W.; Hofmann, H.; Nanoparticles in medicine: Current challenges facing inorganic nanoparticle toxicity assessments and standardizations. *Nanomed.-Nanotechnol. Biol. Med.* **2015**, *11(7)*, 1689-1694. DOI: 10.1016/j.nano.2015.05.005.

(20) Mulla, M.Z.; Rahman, M. R. T.; Marcos, B.; Tiwari, B.; Pathania, S. Poly Lactic Acid (PLA) Nanocomposites: Effect of Inorganic Nanoparticles Reinforcement on Its Performance and Food Packaging Applications. Molecules. 2021, 26(7), 1967. DOI: 10.3390/molecules26071967.

(21) Margarucci, L. M.; Spica, V. R.; Protano, C.; Gianfranceschi, G.; Giuliano, M.; Onofrio, V. D.; Mucci, N.; Valeriani, F.; Vitali, M.; Romano, F.; Potential antimicrobial effects of photocatalytic nanothecnologies in hospital settings. *Ann. Ig. Med. Prev. Comunita* **2019**, *31(5)*, 461-473. DOI: 10.7416/ai.2019.2307.

(22) Wainwright, M.; Photodynamic antimicrobial chemotherapy (PACT). *J. Antimicrob. Chemother.* **1998**, *42(1)*, 13-28. DOI: 10.1093/jac/42.1.13.

(23) Jeong, S. B.; Lee, D. U.; Lee, B. J.; Heo, K. J.; Kim, D. W.; Hwang, G. B.; MacRobert, A. J.; Shin, J. H.; Ko, S. H.; Park, S. H.; Oh, Y. S.; Kim, S. J.; Lee, D. Y.; Lee, S. B.; Park, I.; Kim, S. B.; Han, B.; Jung, J. H.; Choi, D. Y.; Photobiocidal-triboelectric nanolayer coating of photosensitizer/silica-alumina for reusable and visible-light-driven antibacterial/antiviral air filters. *Chem. Eng. J.* **2022**, *440(15)*, 135830. DOI: 10.1016/j.cej.2022.135830.

(24) Page, K.; Correia, A.; Wilson, M.; Allan, E.; Parkin. I. P.; Light-activated antibacterial screen protectors for mobile telephones and tablet computers. *Photochem. Photobiol. A-Chem.* **2015**, *296(1)*, 19-24. DOI: 10.1016/j.jphotochem.2014.08.011.

(25) Khaligh, A.; Khan, R.; Akolpoğlu Başaran, D. D.; Özkan, M.; Tuncel, D.; Photoactive Catalytically Self-Threaded 2D Polyrotaxane Network for Visible Light Activated Antimicrobial Phototherapy. *ACS Appl. Polym. Mater.* **2020**, *2(12)*, 5726-5734. DOI: 10.1021/acsapm.0c01010

(26) Bozja, J.; Sherrill, J.; Michielsen, S.; Stojiljkovic, I.; Porphyrin‐based, light‐activated antimicrobial materials. *J. Polym. Sci. A Polym. Chem.* **2003**, *41(15)*, 2297-2303. DOI: 10.1002/pola.10773

(27) Heo, K. J.; Jeong, S. B.; Shin, J.; Hwang, G. B.; Ko, H. S.; Kim, Y.; Choi, D. Y.; Jung, J. H.; Water-repellent TiO2-organic dye-based air filters for efficient visible-light-activated photochemical inactivation against bioaerosols. *Nano Lett*. **2020**, *21(4)*, 1576-1583. DOI: 10.1021/acs.nanolett.0c03173.

(28) Hwang, G. B.; Huang, H.; Wu, G.; Shin, J.; Kafizas, A.; Karu, K.; Toit, H. D.; Alotaibi, A. M.; Mohammad-Hadi, L.; Allan, E.; MacRobert, A. J.; Gavriilidis, A.; Parkin. I. P.; Photobactericidal activity activated by thiolated gold nanoclusters at low flux levels of white light. *Nat. Commun*. **2020**, *11(1)*, 1207. DOI: 10.1038/s41467-020-15004-6.

(28) Hwang, G. B.; Huang, H.; Wu, G.; Shin, J.; Kafizas, A.; Karu, K.; Toit, H. D.; Alotaibi, A. M.; Mohammad-Hadi, L.; Allan, E.; MacRobert, A. J.; Gavriilidis, A.; Parkin. I. P.; Photobactericidal activity activated by thiolated gold nanoclusters at low flux levels of white light. *Nat. Commun*. **2020**, *11(1)*, 1207. DOI: 10.1038/s41467-020-15004-6.

(29) Lee, S.; Lee, N.; Patel, K. D.; Jun, S.; Park, J.; Knowles, J. C.; Kim, H. ; Lee H.; Lee, J.; A Study on Myogenesis by Regulation of Reactive Oxygen Species and Cytotoxic Activity by Selenium Nanoparticles, *Antioxidants*, **2021**, *10*, 1727. DOI: 10.3390/antiox10111727

(30) Voutsas, A. T.; A new era of crystallization: advances in polysilicon crystallization and crystal engineering. *Appl. Surf. Sci.* **2003**, 208-209(15): 250-262. DOI: 10.1016/S0169-4332(02)01343-0.

(31) Sugimoto, Y.; Takata, N.; Hirota, T.; Ikeda, K. I.; Yoshida, F.; Nakashima, H.; Nakashima, H.; Low-temperature fabrication of polycrystalline Si thin film using Al-induced crystallization without native Al oxide at amorphous Si/Al interface. *Jpn. J. Appl. Phys.* **2005**, *44(7R)*, 4770. DOI: 10.1143/JJAP.44.4770.

(32) Eisenreich, N.; Fietzek, H.; Juez-Lorenzo,M. D. M.; Kolarik, V.; Koleczko, A.; Weiser. V.; On the mechanism of low temperature oxidation for aluminum particles down to the nano-scale. *Propellants Explos. Pyrotech.* **2004**, *29(3)*, 137-145. DOI: 10.1002/prep.200400045.

(33) Liu, J.; Wang, Y.; An, L.; Abnormal behavior of silica doped with small amounts of aluminum. *Sci. Rep.* **2016**, *6(1)*, 1-6. DOI: 10.1038/srep35556.

(34) Herth, E.; Zeggari, R.; Rauch, J.; Remy-Martin, F.; Boireau, W.; Investigation of amorphous SiOx layer on gold surface for Surface Plasmon Resonance measurements. Microelectron. Eng. 2016, 163(1) 43-48. DOI: 10.1016/j.mee.2016.04.014.

(35) Olivieri, G.; Cossaro, A.; Capria, E.; Benevoli, L.; Coreno, M.; Simone, M. D.; Prince, K. C.; Kladnik, G.; Cvetko, D.; Fraboni, B.; Morgante, A.; Floreano, L.; Fraleoni-Morgera, A.; Intermolecular hydrogen bonding and molecular orbital distortion in 4-hydroxycyanobenzene investigated by X-ray spectroscopy. *J. of Phys. Chem. C*, **2015**, *119(1)*, 121-129. DOI: 10.1021/jp5100878.

(36) Rytwo, G.; Zakai, R.; Wicklein, B.; The Use of ATR-FTIR Spectroscopy for Quantification of Adsorbed Compounds. *J. Spectrosc.* **2015**, *2015*, 727595. DOI: 10.1155/2015/727595.

(37) Zhou, S.; Zheng, X.; Yu, X.; Wang, J.; Weng, J.; Li, X.; Feng, B.; Yin, M.; Hydrogen Bonding Interaction of Poly(d,l-Lactide)/hydroxyapatite Nanocomposites. *Chem. Mat.* **2007**, *19(2)*, 247-253. DOI: 10.1021/cm0619398.

(38) Cintrón, M. S.; Hinchliffe, D. J.; FT-IR examination of the development of secondary cell wall in cotton fibers. *Fibers* **2015**, *3(1)*, 30-40. DOI: 10.3390/fib3010030.

(39) Lee, C. M.; Kubicki, J. D.; Fan, B.; Zhong, L.; Jarvis, M. C.; Kim, S. H.; *J. Phys. Chem. B* **2015**, *119(49)*, 15138-15149. DOI: 10.1021/acs.jpcb.5b08015.

(40) Li, L.; Chan, C.; Weng, L.; The effects of specific interactions on the surface structure and composition of miscible blends of poly (vinyl alcohol) and poly (N-vinyl-2-pyrrolidone). *Polymer* **1998**, *39(11)*, 2355-2360. DOI: 10.1016/S0032-3861(97)00534-X.

(41) Sullivan, T. M.; Middleman, S.; Film thickness in blade coating of viscous and viscoelastic liquids. *J. Non-Newton. Fluid Mech.* **1986**, *21(1)*, 13-38. DOI: 10.1016/0377-0257(86)80060-X.

(42) Tait, J. G.; Merckx, T.; Li, W.; Wong, C.; Gehlhaar, R.; Cheyns, D.; Turibiez, M.; Heremans, P.; Determination of solvent systems for blade coating thin film photovoltaics. *Adv. Funct. Mater.* **2015**, *25(22)*, 3393-3398. DOI: 10.1002/adfm.201501039.

(43) Xiao, Y.; Zuo, C.; Zhong, J.; Wu, W.; Shen, L.; Ding, L.; Large-Area Blade-Coated Solar Cells: Advances and Perspectives. *Adv. Energy Mater.* **2021**, *11(21)*, 2100378. DOI: 10.1002/aenm.202100378.

(44) Khaliq, S.; Abbas, Z.; Theoretical analysis of blade coating process using simplified Phan-Thien-Tanner fluid model: an analytical study. *Polym. Eng. Sci.* **2021**, *61(1)*, 301-313. DOI: 10.1002/pen.25576.

(45) Abbas, Z.; Khaliq, S.; Variation of coating thickness in blade coating process of an upper-convected Jeffery's fluid model. *Iran. Polym. J.* **2022**, *31(3)*, 343-355. DOI: 10.1007/s13726-021-01002-y.

(46) Gennes, P.; Brochard-Wyart, F.; Quéré, D.; Hydrodynamics of Interfaces in *Capillarity and wetting phenomena: drops, bubbles, pearls, waves*, Springer New York, 2004; pp 107-138.

(47) Hwang, G. B.; Elaine, A.; Ivan P. P.; White light-activated antimicrobial paint using crystal violet. *ACS Appl. Mater. Interfaces* **2016**, *8(24)*, 15033-15039. DOI: 10.1021/acsami.5b06927

(48) Noimark, S.; Salvadori, E.; Gómez-Bombarelli, R.; MacRobert, A. J.; Parkin, I. P.; Kay, C. W. M.; Comparative study of singlet oxygen production by photosensitiser dyes encapsulated in silicone: towards rational design of anti-microbial surfaces. *Phys. Chem. Chem. Phys.* **2016**, *18(40)*, 28101-28109. DOI: 10.1039/C6CP02529C.

(49) Sehmi, S. K.; Noimark, S.; Bear, J. C.; Peveler, W. J.; Bovis, M.; Allan, E.; MacRobert, A. J.; Parkin. I. P.; Lethal photosensitisation of Staphylococcus aureus and Escherichia coli using crystal violet and zinc oxide-encapsulated polyurethane. *J. Mat. Chem. B.* **2015**, *3(31)*, 6490-6500. DOI: 10.1039/C5TB00971E.

(50) Wang, K.; Song, S.; Jung, S.; Hwang, J.; Kim, M.; Kim, J.; Sung, J.; Lee. J.; Kim, Y.; Lifetime and diffusion distance of singlet oxygen in air under everyday atmospheric conditions. *Phys. Chem. Chem. Phys.* **2020**, *22(38)*, 21664-21671. DOI: 10.1039/D0CP00739K.

(51) Wen, J.; Li, X.; Liu, W.; Fang, Y.; Xie, J.; Xu, Y.; Photocatalysis fundamentals and surface modification of TiO_2 nanomaterials. *Chin. J. Catal.* **2015**, *36(12)*, 2049-2070. DOI: 10.1016/S1872-2067(15)60999-8.

(52) Patir, A.; Hwang, G. B.; Lourenco, C.; Nair, S. P.; Carmalt, C. J.; Parkin, I. P.; Crystal Violet-Impregnated Slippery Surface to Prevent Bacterial Contamination of Surfaces. *ACS Appl. Mater. Interfaces* **2021**, 13(4): 5478-5485. DOI: 10.1021/acsami.0c17915.

(53) Hirose, M.; Yoshida, Y.; Horii, K.; Hasegawa, Y.; Shibuya, Y.; Efficacy of antimicrobial photodynamic therapy with Rose Bengal and blue light against cariogenic bacteria. *Arch. Oral Bio.* **2021**, *122*, 105024. DOI: 10.1016/j.archoralbio.2020.105024.

(54) Fu, G.; Vary, P. S.; Li, C.; Anatase TiO_2 nanocomposites for antimicrobial coatings. *J. Phys. Chem. B.* **2005**, *109(18)*, 8889-8898. DOI: 10.1021/jp0502196.

(55) Hwang, G. B.; Patir, A.; Allan, E.; Nair, S. P.; Parkin, I. P.; Superhydrophobic and white light-activated bactericidal surface through a simple coating. *ACS Appl. Mater. Interfaces.* **2017**, *9(34)*, 29002-29009. DOI: 10.1021/acsami.7b05977.

(56) Choi, D. Y.; Heo, K. J.; Kang, J.; An, E. J.; Jung, S. H.; Lee, B. U.; Lee, H. M.; Jung, J. H.; Washable antimicrobial polyester/aluminum air filter with a high capture efficiency and low pressure drop. *J. Hazard. Mater.* **2018**, *351(5)*, 29-37. DOI: 10.1016/j.jhazmat.2018.02.043.

(57) Zhang, J.; Li, B.; Wu, L.; Wang, A.; Facile preparation of durable and robust superhydrophobic textiles by dip coating in nanocomposite solution of organosilanes. *Chem. Commun.* **2013**, *49(98)*, 11509-11511. DOI: 10.1039/C3CC43238F.

(58) Choi, D. Y.; Kim, M. H.; Oh, Y. S.; Jung, S. H.; Jung, J. H.; Sung, H. J.; Lee, H. W.; Lee. H. M.; Highly stretchable, hysteresis-free ionic liquid-based strain sensor for precise human motion monitoring. *ACS appl. Mater. Interfaces.* **2017**, *9(2)*, 1770-1780. DOI: 10.1021/acsami.6b12415.

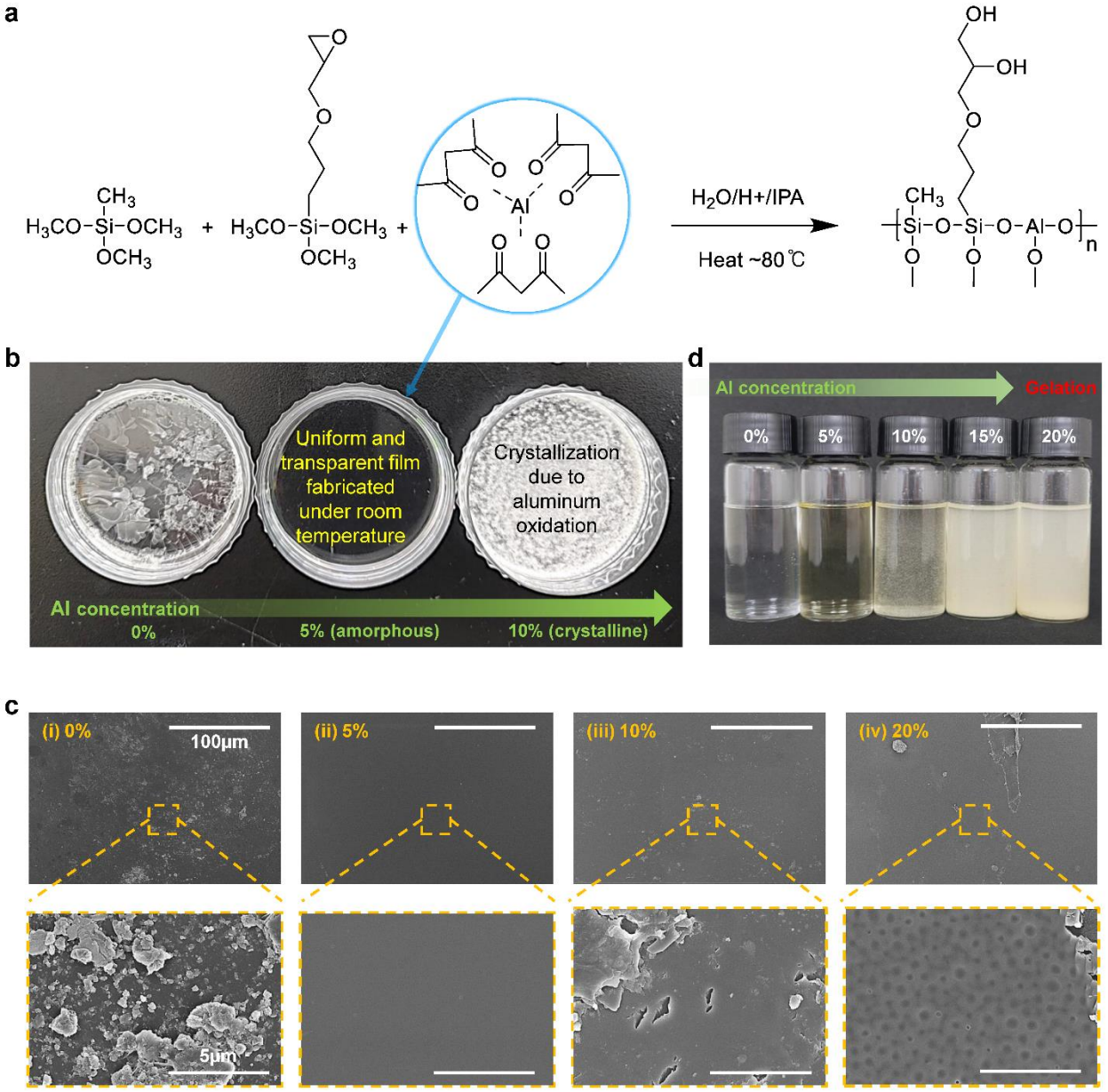

Figure 1. The effect of aluminum sol addition. (a) Schematic of the Si-Al synthesis process. (b) Effect of Al concentration on transparent film fabrication at room temperature. (c) Scanning electron microscopy of Si-Al film images according to Al concentrations. (d) Digital image of Si-Al solution according to Al concentration.

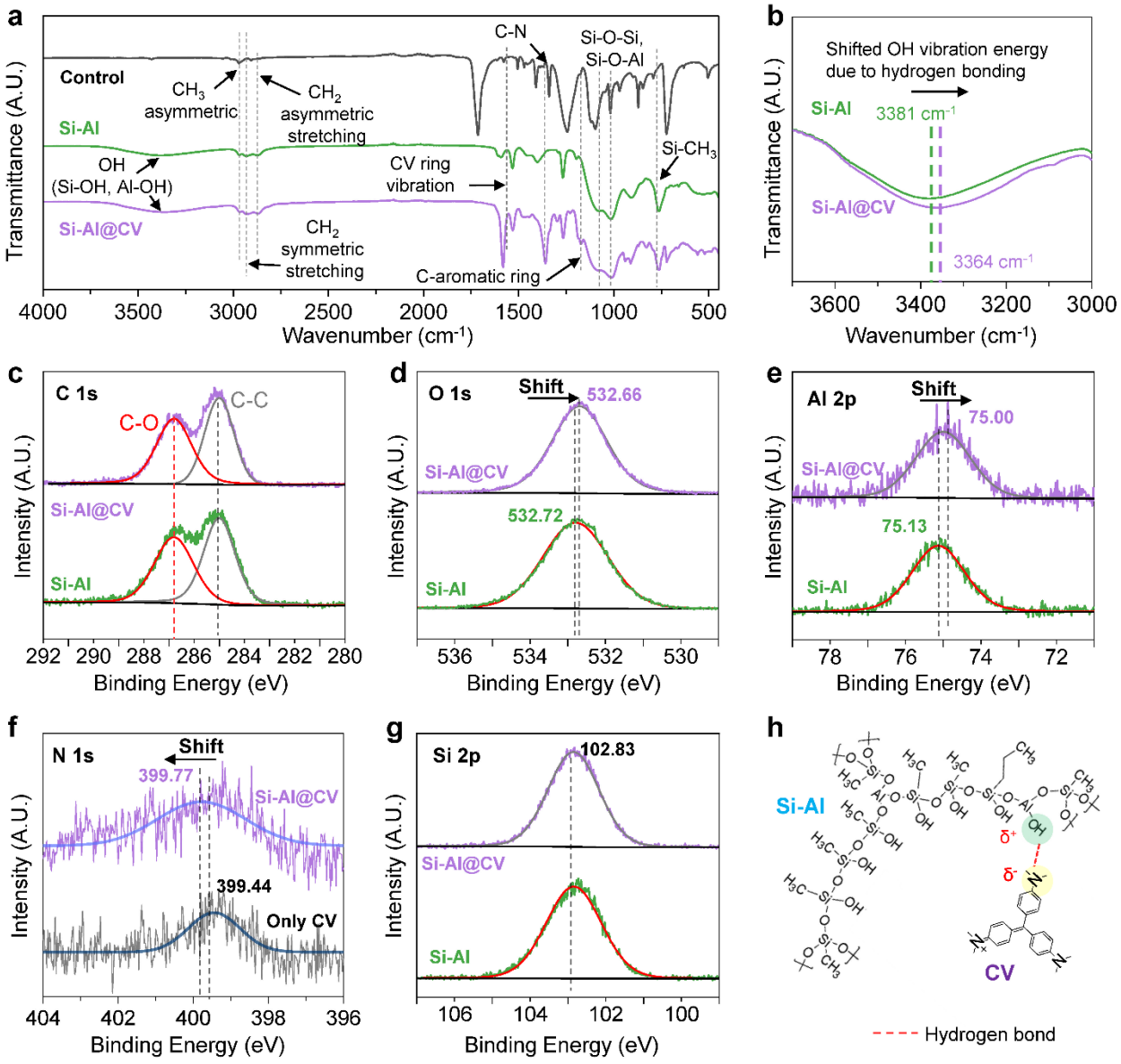

Figure 2. Investigation of hydrogen bonding between Si-Al and CV via FT-IR and XPS measurements. (a) The FTIR spectra of control, Si-Al, and Si-Al@CV film. (b) Magnified FTIR spectra of Si-Al and Si-Al@CV in the OH vibration energy region. (c) C 1s, (d) O 1s, (e) Al 2p and (g) Si 2p scans of Si-Al and Si-Al@CV film. (f) N 1s scan of Si-Al@CV and CV film. (h) Schematic diagram of the chemical structure of Si-Al@CV and the mechanism of CV immobilization by hydrogen bonding.

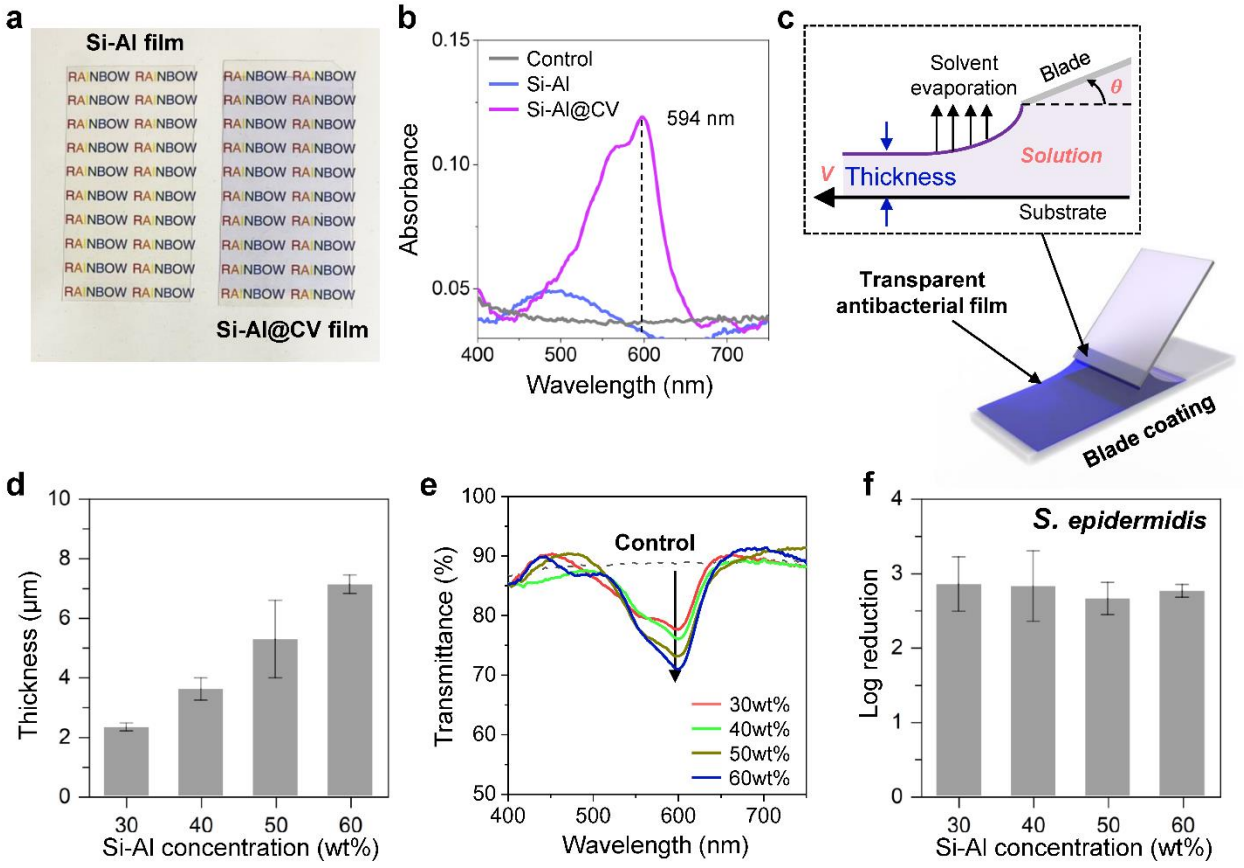

Figure 3. Transparent antibacterial Si-Al@CV film. (a) Digital image of the transparent antibacterial film. (b) UV-vis spectra of control, Si-Al and Si-Al@CV film. (c) Schematic diagram of the blade coating method. (d) Film thickness and (e) transmittance of Si-Al@CV film at different Si-Al concentrations. (f) The antibacterial performance against *S. epidermidis* after 6 h of visible light irradiation. All samples were prepared with a CV concentration of 1 mM.

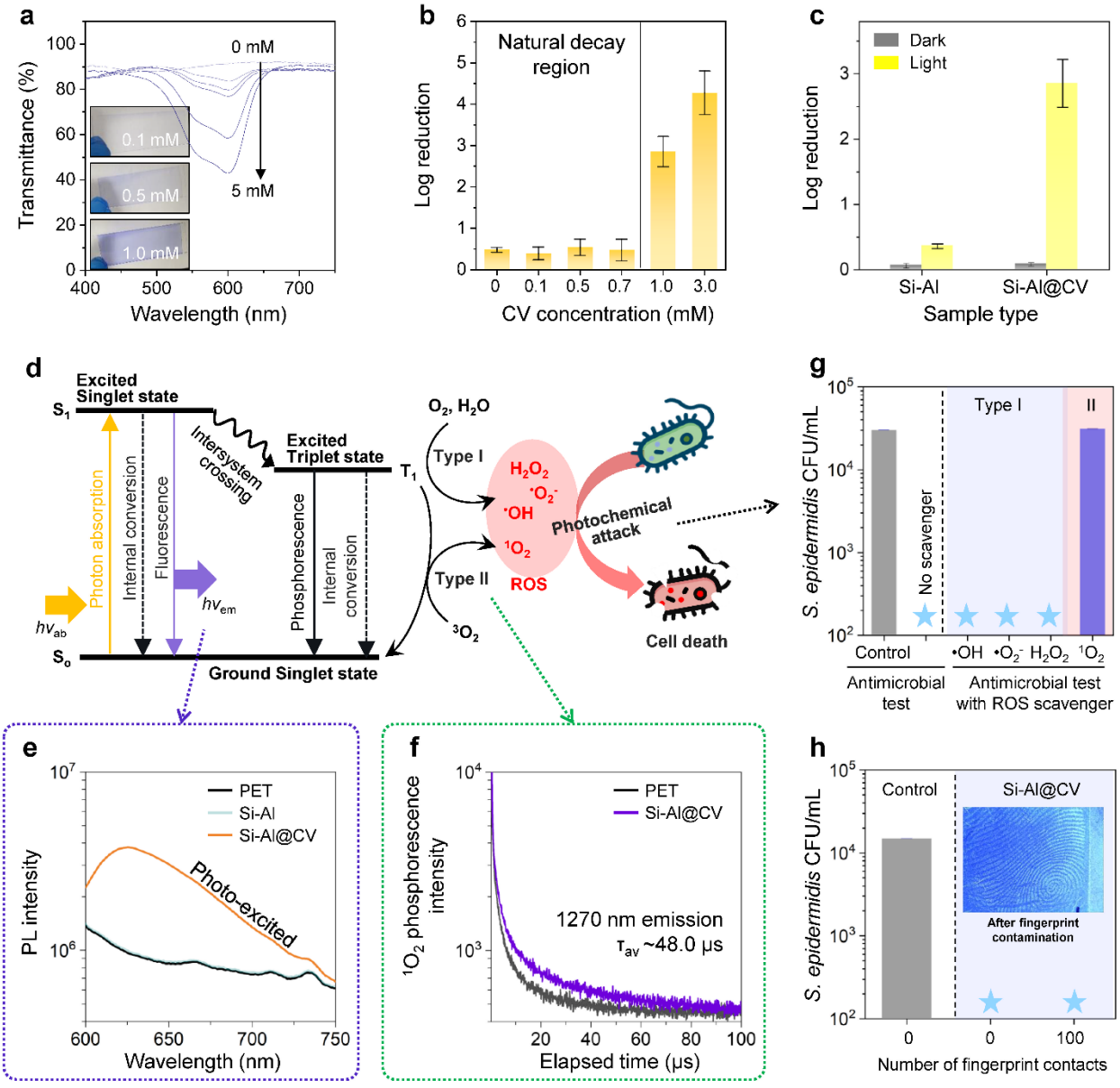

Figure 4. Antibacterial performance and underlying mechanism of Si-Al@CV. (a) The transmittance of Si-Al@CV as a function of CV concentration. (b) Visible-light-activated antibacterial performance against *S. epidermidis* according to the CV concentration. (c) Antibacterial performance of Si-Al@CV film with 1mM CV against *S. epidermidis* after 6h with or without light. (d) Photochemical antibacterial mechanism of the CV under light conditions. (e) Photoluminescence spectra of the control, Si-Al, and Si-Al@CV at a wavelength of 600 to 800 nm (λ_{Ex} = 540 nm). (f) Time-resolved $^1O_2$ phosphorescence decay for the PET and Si-Al@CV film. (g) Bacterial inactivation according to scavenger quenching conditions. (h) Photochmical antibacterial activity of Si-Al@CV after fingerprint contamination. The inset image shows the Si-

Al@CV film surface after fingerprint contamination. Blue stars represent below detection limit: $<10^2$ CFU mL^{-1}.

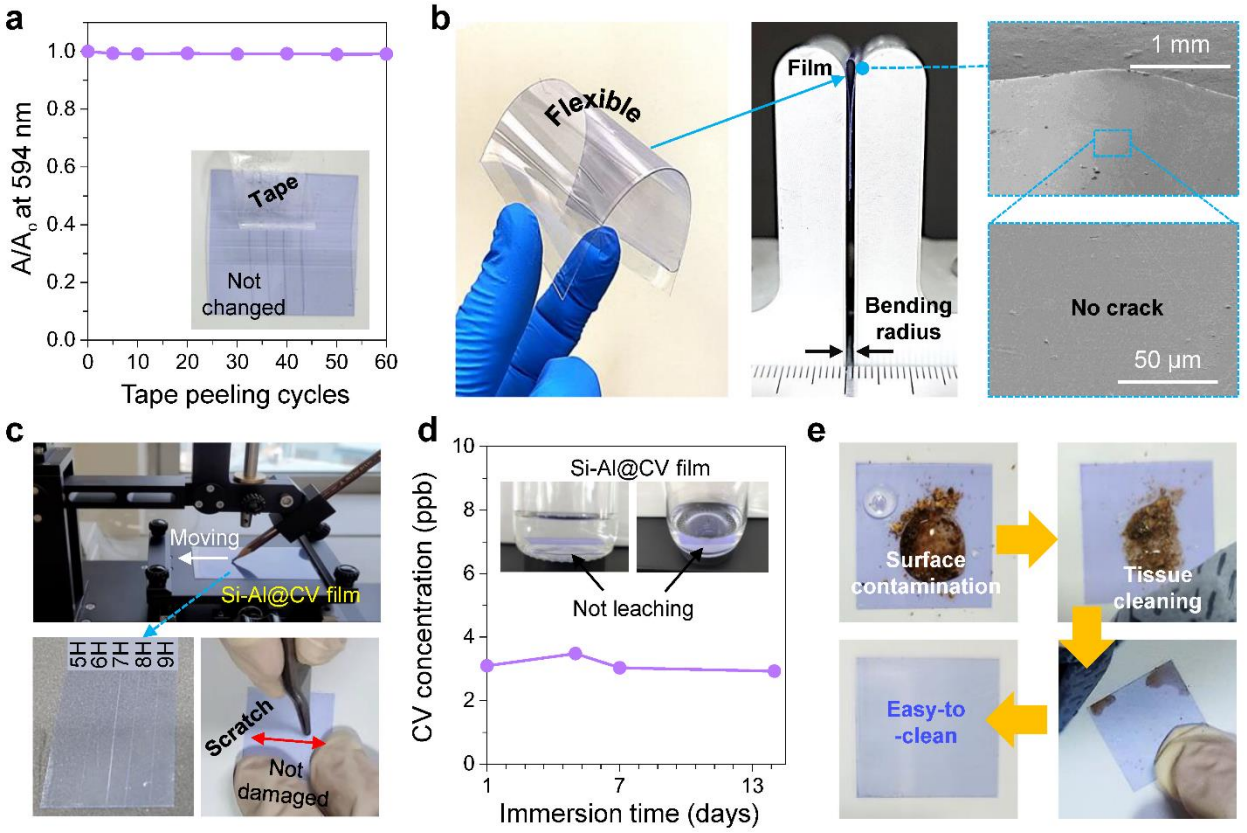

Figure 5. Mechanical stability test. (a) Tape peeling test, (b) bending test and (c) pencil hardness test. (d) Leaching of CV from the Si-Al@CV surface. The inset image shows the leaching solution from Si-Al@CV film after 14 days. (e) Demonstration of the ease of cleaning with a tissue wipe. The surface is contaminated by water with coarse sand grains (1-2 mm in size).

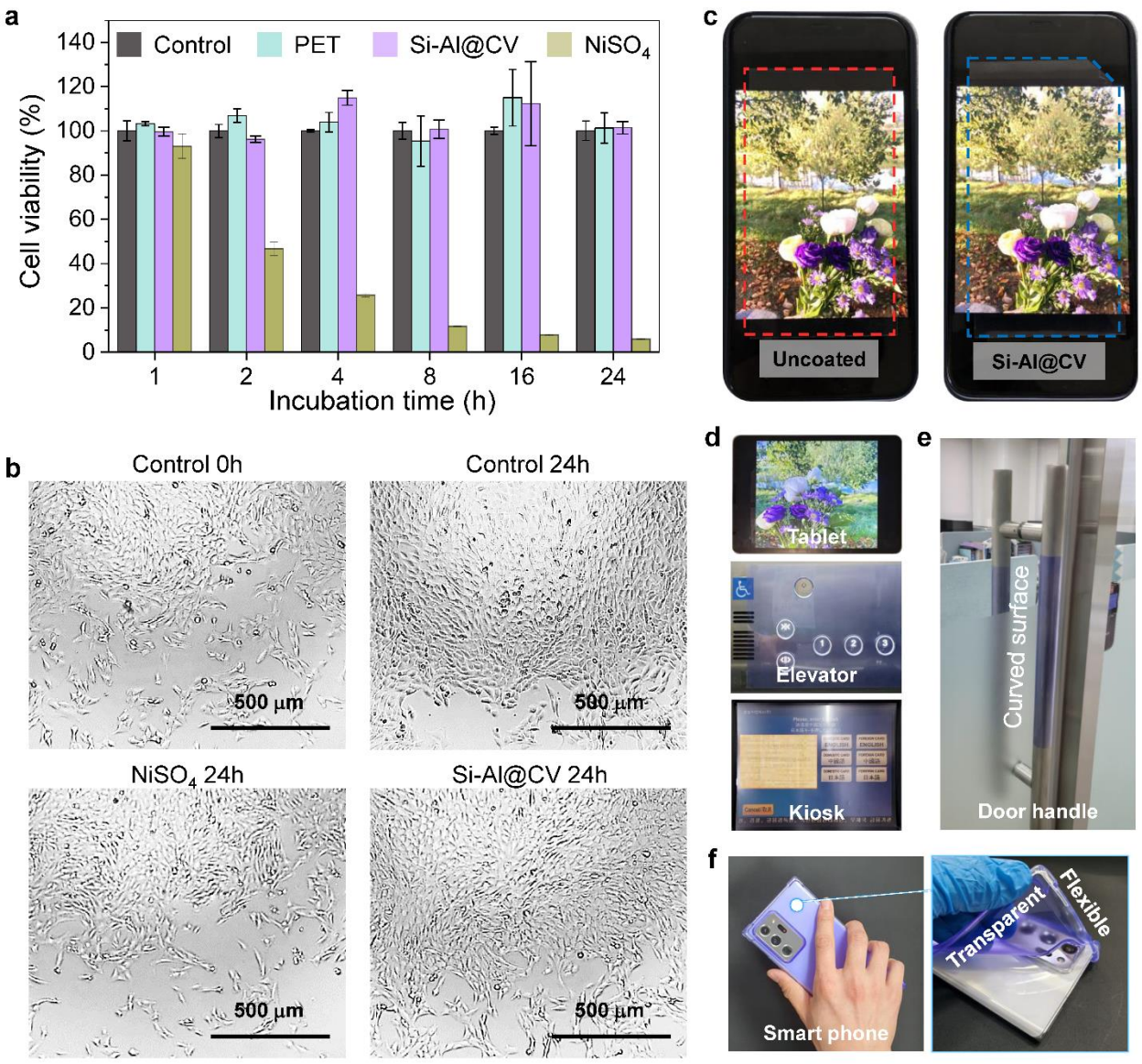

Figure 6. Cytotoxicity tests of Si-Al@CV film. (a) Cell viability and (b) optical cell images of C2C12 myoblast depending on the exposure time. (c) A Si-Al@CV film with the touch screen on the smartphone (iPhone 12 Pro). (d) Demonstration of application of scaled-up Si-Al@CV film to the tablet (iPad Pro 12.9) (top), elevator control panel (middle), and touch screen kiosk (bottom). (e) Photographs of the Si-Al@CV films on the curved door handle surface. (f) A smartphone case with Si-Al@CV coating via air spray coating method.

Table of Contents (TOC)